



Hotter and drier climate made the Mediterranean Europe and Northern Africa region a shrubbier landscape

Wei Fang^{1,2} · Chuixiang Yi^{2,3} · Deliang Chen⁴ · Peipei Xu^{2,5} · George Hendrey^{2,3} · Nir Krakauer^{3,6} · Katherine Jensen^{3,6} · Shan Gao^{2,7} · Zihan Lin⁸ · Gabriella Lam¹ · Qin Zhang^{2,9} · Tao Zhou¹⁰

Received: 5 February 2021 / Accepted: 11 September 2021
© The Author(s), under exclusive licence to Springer-Verlag GmbH Germany, part of Springer Nature 2021

Abstract

A shift to higher temperatures has left the Mediterranean Europe and Northern Africa (MENA) region more vulnerable to drought and land degradation. We used MODIS LAI (leaf area index) and GPP (gross primary production) deficits, the differences between actual and historical-maximum values, to describe vegetation structural and functional changes and consequential landcover change in response to changing climate conditions during 2001–2019 in the area (20° W–45° E, 20° N–45° N). We found that 1) the vegetation responses varied significantly among eight landcover types with the decreasing importance: forests, savannas, a mosaic of cropland and natural vegetation (CNV), croplands, permanent wetlands, urban land, grasslands, and shrublands, each with distinctive yet overlapping signatures over the ranges of the climate conditions considered. 2) Forests, occupying the coolest and wettest niche, showed the strongest response to severe drought with a lag of 1–3 years and a legacy effect for 10 years. Shrubs, occupying the hottest and driest niche, were the most resilient under a hotter and drier climate. 3) The total areas of savannas and CNV increased by 394,994 and 404,592 km², respectively, while that of forests decreased by 33,091 km². Shrublands extended by 287,134 km² while grasslands and croplands retreated by 490,644 and 225,263 km². The area of wetlands increased by 49,192 km², and that of urban land increased by 39,570 km². A total of 57,649 km² of barren land became vegetated over the years. Along with higher temperature and more extended period of drought, MENA has evolved towards a shrubbier landscape.

Keywords LAI deficit · GPP deficit · Climate drivers · Legacy effect · Landcover transition

Introduction

Landcover, especially vegetation dynamics over land, plays a critical role in atmospheric processes and the water and carbon cycles globally (Foley et al. 1996; Sitch et al. 2003;

Assal et al. 2016). An analysis of FLUXNET data revealed that the exchanges of carbon, water, and energy between terrestrial ecosystems and the atmosphere are limited primarily by water availability when the mean annual temperature is above a threshold of 16 °C (Yi et al. 2010). Climate records from the past 6 decades show that the annual mean temperature of a significant part of the Mediterranean, Europe, and

Communicated by Paul Stoy.

✉ Chuixiang Yi
chuixiang.yi@qc.cuny.edu

¹ Department of Biology, Pace University, New York, NY 10038, USA

² School of Earth and Environmental Sciences, Queens College, City University of New York, Flushing, NY 11367, USA

³ The Graduate Center, City University of New York, New York, NY 10016, USA

⁴ Department of Earth Sciences, University of Gothenburg, 40530 Gothenburg, Sweden

⁵ School of Geography and Tourism, Anhui Normal University, Wuhu 241002, China

⁶ The City College of New York, City University of New York, New York, NY 10031, USA

⁷ Institute of Tibetan Plateau Research, Chinese Academy of Sciences, Beijing 100101, China

⁸ Center for Global Change and Earth Observations, Michigan State University, East Lansing, MI 48823, USA

⁹ Dalian University of Technology, Dalian 116024, China

¹⁰ Faculty of Geographical Science, Beijing Normal University, Beijing 100875, China

Northern Africa (MENA) region have shifted from below to above this temperature threshold (Yi et al. 2014; Allen et al. 2015; Huang et al. 2015). This shift to higher temperatures has left the largely arid and semiarid MENA region more vulnerable to drought and land degradation (Somot et al. 2008; Segui et al. 2010; Friend 2010; IPCC 2013; Zhang et al. 2020; Peñuelas and Sardans 2021). Indeed, some studies have reported drought-induced forest impacts and die-backs in the Mediterranean region (Allen et al. 2010; Carnicer et al. 2011; Peñuelas et al. 2001; Martínez-Vilalta and Piñol 2002; Matusick et al. 2013), as well as shifts in vegetation composition (Jump and Peñuelas 2005; Anderegg et al. 2012).

The drivers of changing vegetation patterns are complex, and human activity as well as climate change is involved (Alexandrian et al. 1998). Indeed, changing climate is clearly linked to changes in human land use in the MENA region (Cramer et al. 2018). However, in this study, we seek to identify statistical correlations between patterns of vegetation and climate in the MENA region. Climate is a strong contributor to variability and change of vegetation and is a matter of both ecological and economic concern, as strong sensitivity to climate can result in rapid land use change (Vanacker et al. 2005; Serra et al. 2008a, b). Over longer time scales, relatively small shifts in background climate can impact the distribution of ecosystems and potentially the viability of agricultural and pastoral systems (Ciais et al. 2005; Vicente-Serrano et al. 2012a, b). Interest in the climate sensitivities of vegetation in semiarid regions is evident in the substantial body of research devoted to characterizing the relationships between precipitation, soil type, land management, and vegetation growth in these water-stressed regions (Zaitchik et al. 2007; Vicente-Serrano et al. 2012a, b). Previous studies have shown that, since 1948, a warmer climate has moved the 16 °C isotherm poleward, leading to a predicted northward shift of vegetation distribution of the Northern hemisphere (Yi et al. 2014). Vicente-Serrano et al. (2012a, b) also showed a decline of the average vegetation cover in the semiarid Mediterranean environments during 1984–2008.

At regional to continental scales, satellite observation offers a feasible and effective approach for monitoring vegetation dynamics. One of the most common observations of vegetation dynamics is based on the normalized difference vegetation index (NDVI). The NDVI, computed as a normalized ratio of reflectance in the near-infrared and red portions of the electromagnetic spectrum, provides a measure of chlorophyll abundance at the Earth's surface and offers an indirect measure of energy absorption and vegetation density (Myneni et al. 1995a, b; Kerr and Ostrovsky 2003).

Several vegetation indices with direct ecological meanings are derived from NDVI using additional algorithms and information. One of them is the leaf area index (LAI). LAI

is a fundamental parameter that reflects vegetation structure involved in the processes of fixing atmospheric CO₂ into organic matter. LAI is defined as the one-sided green leaf area per unit ground area in broadleaf canopies and as half the total needle surface area per unit ground area in coniferous canopies. Another widely used vegetation index is gross primary production (GPP), which is a measure of vegetation function in the processes of fixing atmospheric CO₂ into organic matter. GPP correlates closely with LAI where LAI is ~4 or less, suggesting that leaf area is a critical determinant of GPP in most of the MENA region (Chapin et al. 2011).

This study took advantage of interannual climatic variability during 2001–2019 (Sprintsin et al. 2009; Fischer and Knutti 2015) to characterize the climatic sensitivities of vegetation in the MENA region. We applied the “perfect deficit” approach (Yi et al. 2012) to identify the primary climatic drivers of LAI variability over vegetation across the entire MENA domain aggregated by landcover class.

We used both LAI deficit and GPP deficit as direct measures of climate and non-climate stress on ecosystem structure and function experienced by the vegetation of the semiarid MENA area. We focused on climate stress expressed by some climate indices describing thermal and water conditions and their combined effects. We attempted to establish empirical connections of LAI deficit and GPP deficit with a few climate variables/indices (i.e. annual average temperature (T), annual average precipitation (mm), Dryness Index, Temperature–Precipitation (TP) Index, and Standardized Precipitation–Evapotranspiration Index (SPEI)). Our aim was to understand how landcover changes, especially vegetation structural and functional changes and variabilities, respond to these climate variables: Specifically, we examined which of these variable(s) are the dominant driver(s) for the interannual variability of LAI and GPP deficit. When vegetation types were considered individually, we hypothesized that LAI deficit and GPP deficit of different vegetation types would respond to climate variables differently, and that the distribution of vegetation types may extend or shrink in response to climate change. The direction and intensity of a possible landcover shift were further explored with landcover transition matrices. Such ecological assessment at the temporal scale of decades is much needed for the strategic planning of resource management, for optimizing vegetation productivity and ecosystem services.

Materials and methods

Climate and remote sensing data

We collected remote sensing data such as MODIS LAI, GPP and landcover, and various climate measures for the

MENA region, defined as the bounding box of 20° N–45° N and 20° W–45° E. This is a box-shaped area around the Mediterranean Forests, Woodlands & Scrub biome defined by the World Wide Fund for Nature (WWF) in the MENA region (Fig. 1).

For the remote sensing datasets of LAI and GPP suitable for this study, we compared the spatial resolution across all available products for the study area and noticed that 500 m was the highest spatial resolution with continuous time series coverage. Using LAI as an example, there are alternative datasets such as the NOAA CDR AVHRR LAI FAPAR: Leaf Area Index and Fraction of Absorbed Photosynthetically Active Radiation, Version 5 and GCOM-C/SGLI L3 Leaf Area Index (V2). However, the spatial resolution of the NOAA dataset is 0.05 degree, approximately 5.5 km while that of the GCOM-C/SGLI is 2.5 arc minutes, which is about 4.58 km. Both are much coarser than what we employed. Given the large size of our study area, the pixel size of 500 m is assumed to convey sufficient information to address our research questions.

Although the mosaic of plant communities also responded to local geologic, topographic and soil heterogeneity, for which a finer resolution of 1–100 m landcover dataset might be more appropriate, a coarser landcover dataset with 500 m resolution would suffice for our focus on vegetation-climate-vegetation interactions and feedback loops in this paper.

Remote sensing data

We used 19 years (01-Jan-2001–31-Dec-2019) of global 8-day composite MODIS LAI (MODIS/006/MOD15A2H),

GPP (MODIS/006/MOD17A2H), and yearly landcover data (MODIS/006/MCD12Q1) at 500 m resolution from the NASA Land Processes Distributed Active Archive Center (LP DAAC), USGS/Earth Resources Observation and Science (EROS) Center within Google Earth Engine. Annual landcover classification is defined with the International Geosphere Biosphere Programme (IGBP) global vegetation classification scheme. It describes the landcover properties derived from observations spanning a year of Terra and Aqua MODIS data. The primary landcover scheme identifies 17 landcover classes defined by IGBP, which includes 11 natural vegetation classes, 3 developed and mosaicked land classes, and 3 non-vegetated land classes. For our analyses, we grouped these into eight categories of vegetated cover: forests (including class 1–5, evergreen needleleaf forest, evergreen broadleaf forest, deciduous needleleaf forest, deciduous broadleaf forest, and mixed forest), shrublands (including class 6–7, closed shrublands and open shrublands), savannas (classes 8–9 woody savannas and savannas), grasslands (class 10), permanent wetlands (class 11), croplands (class 12), urban and built-up (class 13) and crop + natural vegetation (CNV) mosaic (class 14). Pixels with landcover that changed over the years were coded white in the map (Fig. 1) and were excluded for the no-landcover-change-based analyses along with the non-vegetated areas (including snow and ice-class 15, barren land-class 16 and water-class 17).

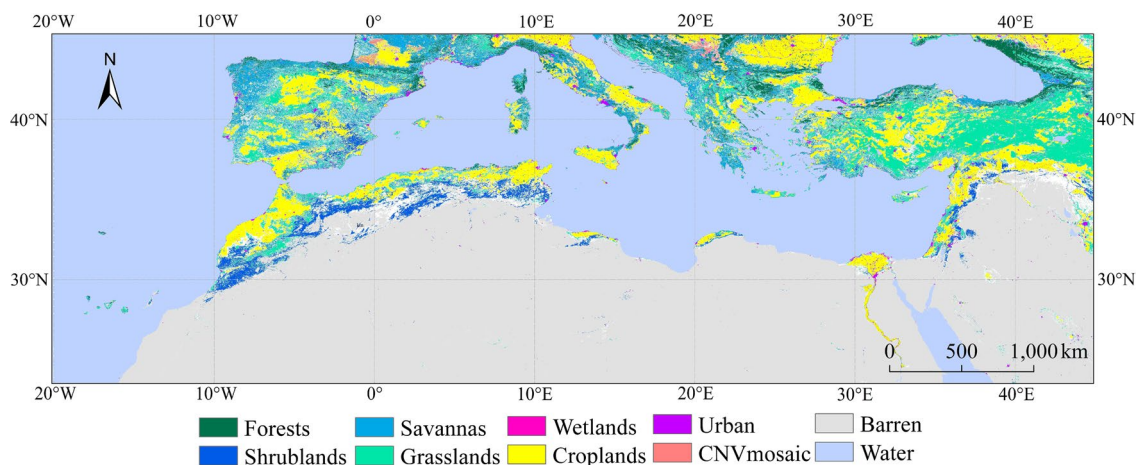


Fig. 1 A map of vegetated areas with no change of landcover types during 2001–2018 (500 m resolution) in Mediterranean Europe and North Africa (MENA, 20° W–45° E and 20° N–45° N). Pixels that experienced landcover change were in white color. Annual landcover classification is defined by the MODIS Landcover CMG (MCD12Q1) product's International Geosphere Biosphere Programme (IGBP) global vegetation classification scheme (https://lpdaac.usgs.gov/products/modis_products_table/mcd12c1).

The primary landcover scheme identifies 17 classes, and were grouped into 8 categories: forests (class 1–5), shrubland (class 6–7), savannas (class 8–9), grasslands (class 10), permanent wetlands (class 11), croplands (class 12), urban and built-up (class 13), and crop + natural vegetation mosaic (class 14). The non-vegetated areas (water and barren land) were excluded from relevant analyses

Climate indices

We chose two primary instrumental measures (temperature and precipitation) and three compound climate indices which transform basic climate variables such as temperature and precipitation in different ways to assess water stress, one with a linear function, one with an exponential function, and one being standardized, for this study.

We used monthly global surface air temperature (average air temperature at 2 m height) and precipitation (monthly sum) data (01-Jan-2001–31-Dec-2019) at 0.25° resolution provided by ECMWF/Copernicus Climate Change Service within Google Earth Engine. The source of these data ERA5 is the fifth generation ECMWF atmospheric reanalysis of the global climate that combines model data with observations from across the world into a globally complete and physically consistent dataset.

To calculate dryness index, we collected monthly average net radiation ($W\ m^{-2}$) data (01-Jan-2001–31-Dec-2019) at 0.1 degree resolution from the FLDAS (Famine Early Warning System Network (FEWS NET) Land Data Assimilation System) dataset (McNally et al. 2017) provided by the NASA GES DISC at NASA Goddard Space Flight Center within Google Earth Engine. This FLDAS dataset uses Noah version 3.6.1 surface model with CHIRPS-6 hourly precipitation that has been down-scaled using the NASA Land Surface Data Toolkit.

We first resampled the radiation data with the same projection system and resolution of the temperature and precipitation data. Net radiation (R_n) is defined as the sum of net shortwave radiation and net longwave radiation in a downward direction.

The dryness index of Budyko (1961) was calculated by:

$$\text{Dryness} = \frac{R_n}{LP}, \quad (1)$$

where R_n ($MJ\ m^{-2}\ year^{-1}$) and P ($mm\ year^{-1}$) are, respectively, monthly mean net radiation and precipitation for each grid cell and L is a constant $2.5\ MJ\ kg^{-1}$, the enthalpy of vaporization. Because temperature is often positively correlated with R_n , dryness increases in response to increasing T or decreasing P . When there is no precipitation in a month, the dryness index value could be infinitely large. On the global-scale the average net radiation was between 98 and $112.6\ W\ m^{-2}$ (Liang 2018) and average precipitation multiplied by L was comparable, therefore, the dryness index values (annual average of the monthly values) were capped under 100 for later analysis.

Temperature–Precipitation (TP) Index was derived initially from a model of soil nitrogen variations (Jenny

1984) and further adapted to model vegetation responses to a changing climate (Yi et al. 1996). It is calculated by:

$$TP = e^{-0.08T}(1 - e^{-0.005P}), \quad (2)$$

where T ($^{\circ}C$) and P ($mm\ year^{-1}$) are annual mean temperature and precipitation for each grid cell, respectively (Yi et al. 1996). TP Index increases in response to decreasing T or increasing P .

SPEI (Standardized Precipitation–Evapotranspiration Index) is a measure of water balance, calculated by the standardization of water deficit D ,

$$D = P - PET, \quad (3)$$

where P ($mm\ year^{-1}$) and PET ($mm\ year^{-1}$) are precipitation and potential evapotranspiration for each grid cell, respectively (Vicente-Serrano et al. 2010). The SPEI can measure drought severity according to its intensity and duration. It can identify the onset and end of drought episodes as well. The SPEI is a standardized variable, and it can, therefore, be compared with other SPEI values over time and space. An SPEI of 0 indicates a value corresponding to 50% of the cumulative probability of D , according to a log-logistic distribution (a continuous probability distribution for a non-negative random variable) of D , over a reference period, while positive values indicate wetter than typical conditions and negative values indicate abnormally dry conditions.

A globally gridded (0.5° resolution) SPEI index calculated from the CRU TS3.23 precipitation and reference evapotranspiration was provided by the SPEI website (<https://digital.csic.es/handle/10261/202305>). The SPEI used in the analyses was at the 12-month temporal scale ending December of the previous year.

Perfects, deficits, and relative deficits

Many large-scale vegetation and landcover studies are formulated as statistical analyses of climatological anomalies. This study took a vegetation-centric approach, focusing on the differences in vegetation performance under optimal and suboptimal conditions.

Yi et al. (2012) introduced a “perfect-deficit” approach for quantifying links between climate extremes and variations in carbon storage. We applied this approach in developing a climate stress indicator based on our MODIS LAI and GPP data in the MENA area, available for every 8-day period throughout a year, then converted to monthly values. For each pixel, the “perfect” LAI value of the month is defined as the maximum LAI value for this month over the 19 years, and the “deficit” LAI value of the month for each year is defined as the difference between the observed

value from the “perfect” value of that month. Therefore, for the entire studied time span (2001–2019) for the i th month,

$$\text{LAI}_{\text{Perfect}}(i) = \text{Maximum}\{\text{LAI}_{\text{Observed}}(i)_{2001}, \text{LAI}_{\text{Observed}}(i)_{2002}, \dots, \text{LAI}_{\text{Observed}}(i)_{2019}\}, \quad (4a)$$

$$\text{GPP}_{\text{Perfect}}(i) = \text{Maximum}\{\text{GPP}_{\text{Observed}}(i)_{2001}, \text{GPP}_{\text{Observed}}(i)_{2002}, \dots, \text{GPP}_{\text{Observed}}(i)_{2019}\}, \quad (4b)$$

and for the i th month of the j th year,

$$\text{LAI}_{\text{Deficit}}(i, j) = \text{LAI}_{\text{Perfect}}(i) - \text{LAI}_{\text{Observed}}(i, j), \quad (5a)$$

$$\text{GPP}_{\text{Deficit}}(i, j) = \text{GPP}_{\text{Perfect}}(i) - \text{GPP}_{\text{Observed}}(i, j). \quad (5b)$$

Essentially, we were looking at how the observed LAI for a given month under suboptimal climate and ecological conditions departed from the highest value observed for that time of the year over the 19 years. The perfect value is presumed to correspond to the optimal growing conditions of climate, edaphic features, and other impinging ecological factors for that particular area.

The monthly LAI or GPP deficit values were first averaged within each year to give us an annual mean deficit for each pixel, then were averaged spatially (pixel by pixel) across each of the landcover classes for each year.

Data analyses

There were four sequential steps of data analyses (Supplementary Fig. 1). Step 1—eight vegetated landcover types with no change over 18 years were extracted to conduct multiple regression analyses; Step 2—regressions of vegetation structural (LAI deficit) and functional (GPP deficit) responses over climate drivers (including temperature, precipitation, TP index, dryness index, and SPEI) were conducted over all vegetated pixels and within each of eight vegetation types; Step 3—results of ten regression analyses and probability density function (PDF) curves of seven variables all pointed to the strong constraints within each vegetation type, which shed new light on landcover changes over the years. Step 4—using the characteristic order along the spectrums of climate variables and vegetation response variables, direction and intensity of landcover change were quantified using time series and transition matrices.

All LAI, GPP, and landcover data were retrieved within Google Earth Engine from MODIS products (MOD15A2 and MOD17A2, MCD12Q1). All climate datasets (global surface air temperature, precipitation, and net shortwave radiation data with temporal resolution of 1 month) were resolved to a common projection at 0.25° resolution. All

annual LAI deficits, annual GPP deficits, and all climate indices were calculated within Google Earth Engine using JavaScript. Because we are looking for long-term large-

scale patterns, all data were aggregated to annual averages of eight landcover types. All processed spatial data were then exported to Geotiff files with WGS84 and 500 m resolution for further statistical tests and graphing in R-Studio (version 1.2.1335). All maps were made in ArcGIS Desktop 10.7.1.11595.

Results

Climate drivers

The first objective of the study was to find the climate indices that the vegetation structure indicator LAI and function indicator GPP responded to the most, and how those relationships vary across different vegetation types. We found that overall LAI deficit was negatively correlated with annual average temperature (Fig. 2a, adjusted $R^2 = 0.529$, $p < 0.001$) and dryness (Fig. 2g, adjusted $R^2 = 0.583$, $p < 0.001$), positively correlated with precipitation (Fig. 2c, adjusted $R^2 = 0.613$, $p < 0.001$), and TP Index (Fig. 2g, adjusted $R^2 = 0.491$, $p < 0.001$), and not correlated with SPEI (Fig. 2i, adjusted $R^2 = 0.007$, $p = 0.155$) (Table 1). Among the eight landcover categories, only forest consistently showed a similar pattern to the overall vegetation structural responses while shrubland showed an opposite trend or no trend.

Similarly, we found GPP deficit of overall vegetation was negatively correlated with annual average temperature (Fig. 2b, adjusted $R^2 = 0.553$, $p < 0.001$) and dryness (Fig. 2h, adjusted $R^2 = 0.615$, $p < 0.001$), positively correlated with accumulative precipitation (Fig. 2d, adjusted $R^2 = 0.548$, $p < 0.001$), TP Index (Fig. 2f, adjusted $R^2 = 0.509$, $p < 0.001$), and weakly with SPEI (Fig. 2j, adjusted $R^2 = 0.041$, $p = 0.007$) (Table 1).

Among all the eight landcover categories: only forest showed an almost consistently similar pattern to the overall vegetation structural responses while shrubland showed an opposite trend or no trend. The only exception was in precipitation. Within each vegetation type, GPP deficit decreased when precipitation increased. In another word, the more precipitation, the less reduction of GPP within each vegetation

Fig. 2 Regressions of vegetation structural (LAI deficit) and functional (GPP deficit) responses over climate drivers including **a, b** annual average temperature ($^{\circ}\text{C}$, T), **c, d** accumulative precipitation (mm, P), **e, f** Temperature–Precipitation (TP) index, **g, h** dryness index, **i, j** Standardized Precipitation Evapotranspiration Index (SPEI) for all vegetated pixels (black lines, solid if $p < 0.01$, dotted if $p > 0.05$) and within each of 8 vegetation types (color coded with 95% confidence intervals in gray); for each panel, probability density function (PDF) curves were plotted with the same scheme of color code, horizontal on the top for the climate variables (T, P, TP index, dryness or SPEI), and vertical on the right for the response variables (LAI or GPP deficit)

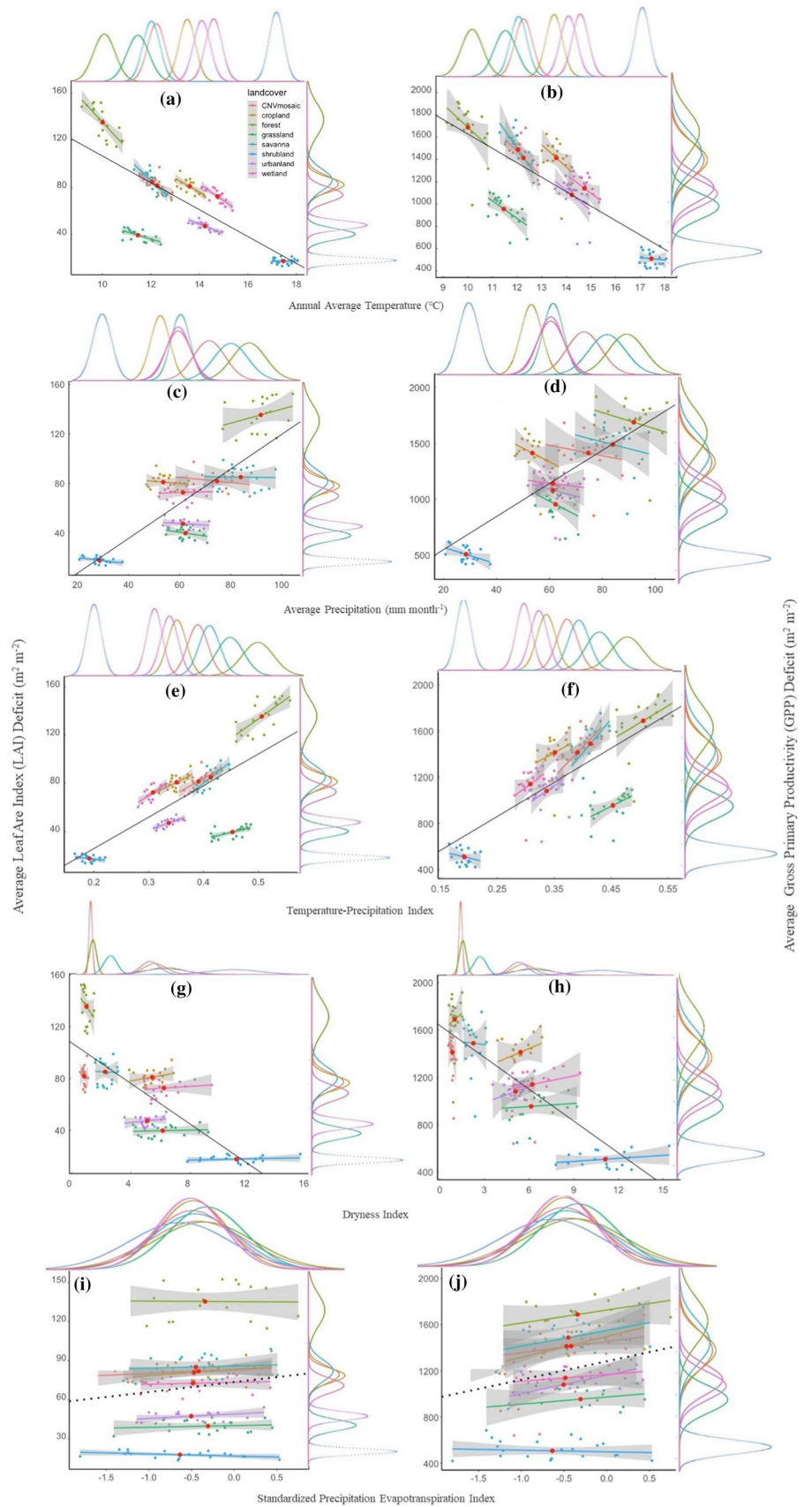


Table 1 Regressions of annual Leaf Area Index (LAI) deficit and gross primary productivity (GPP, in $\text{g C m}^{-2} \text{ year}^{-1}$) deficit over climate drivers

Dependent variable (Y)	Independent variable (X)	Adjusted coefficient of determination (R^2)	Degrees of freedom ($df1, df2$)	Significance (p)	Intercept	Slope
LAI deficit	Temperature	0.53	1,150	<0.0001	220.68	-11.39
	Precipitation	0.61	1,150	<0.0001	-20.77	1.40
	TP index	0.49	1,150	<0.0001	-26.21	260.90
	Dryness index	0.59	1,150	<0.0001	107.35	-7.84
	SPEI	0.01	1,150	0.155	73.48	7.63
GPP deficit	Temperature	0.55	1,151	<0.0001	2925.10	-129.56
	Precipitation	0.55	1,151	<0.0001	255.63	14.77
	TP index	0.51	1,151	<0.0001	122.75	2952.20
	Dryness index	0.62	1, 151	<0.0001	1638.60	-89.64
	SPEI	0.04	1, 151	0.007	1283.74	159.26

TP Index Temperature–Precipitation Index, *SPEI* Standardized Precipitation/Evapotranspiration Index, *LAI* Leaf Area Index, *GPP* gross primary productivity ($\text{gCm}^{-2} \text{ year}^{-1}$)

type as we would normally expect under semiarid climates. The overall correlation between GPP deficit and precipitation was positive.

Landcover-specific signatures over the spectrums of climate conditions

Based on the probability density function (PDF) curves for both dependent variables (i.e. vertical PDF graphs for LAI and GPP deficits) and independent variables (i.e. horizontal PDF graphs for climate indices) (Fig. 3), each vegetation cover demonstrated unique and sometimes overlapping distribution signatures over the span of structural and functional responses, and climate conditions.

For example, forests had by far the highest LAI deficits ($11.3 \pm 1.1 \text{ m}^2 \text{ m}^{-2}$), followed by savannas ($7.1 \pm 0.7 \text{ m}^2 \text{ m}^{-2}$), CNV mosaic ($6.8 \pm 0.6 \text{ m}^2 \text{ m}^{-2}$), croplands ($6.8 \pm 0.5 \text{ m}^2 \text{ m}^{-2}$), wetlands ($6.1 \pm 0.5 \text{ m}^2 \text{ m}^{-2}$), urban land ($3.9 \pm 0.3 \text{ m}^2 \text{ m}^{-2}$), grasslands ($3.3 \pm 0.4 \text{ m}^2 \text{ m}^{-2}$), and shrublands ($1.5 \pm 0.2 \text{ m}^2 \text{ m}^{-2}$) in descending order (Table 2). The LAI deficit of shrublands was less than half of that of grasslands, which was the second lowest among all. Likewise, forests had the highest GPP deficits, followed by the same descending order (Table 2). This order reflected the differential responses, both structural and functional, to these climate variables among these vegetation types, and their differential responses to climate stress.

When looking into the span of climate conditions, stratification of landcover classes by climate conditions is evident in the data record. Forests occupied the coolest ($10.0 \pm 0.5 \text{ }^\circ\text{C}$) and wettest ($1102.3 \pm 87.3 \text{ mm}$) niche while shrublands occurred in the hottest ($17.5 \pm 0.3 \text{ }^\circ\text{C}$) and driest ($342.2 \pm 49.2 \text{ mm}$) area, polar opposite to forests. Each vegetation landcover type is constrained within a limited range

of climate conditions but each has a certain level of overlap with others. Within a constrained range of climate conditions, alternative steady states (vegetation types) may exist.

Landcover change over time

Remotely sensed areal change of landcover

According to the MODIS annual landcover product during 2001–2018, the total areas of savannas and CNV mosaics in MENA increased by $394,994 \text{ km}^2$ (5.3% of savanna area in 2001) and $404,592 \text{ km}^2$ (29.7% of CNV area in 2001), with a significantly steady increasing trend ($R^2=0.930$ and 0.913 , respectively), while the area of forests decreased by $33,091 \text{ km}^2$ (1.6%) (Fig. 3a–c) despite the fertilizer effect of elevated ambient CO_2 .

More specifically, the area identified as forest in this analysis decreased by $41,401 \text{ km}^2$ (a 2.9% drop) over 3 years following the drought/heat wave of 2002, and did not recover to the pre-drought level until 2014, 11 years after the drought. It is unclear whether other droughts (e.g. 2005) also impacted vegetation dynamics and prolonged the recovery. A second major drop happened between 2016 and 2017, leaving an overall areal decline between 2001 and 2018.

Over the 18 years, shrublands, occupying the hottest and driest niche of MENA, extended by $287,134 \text{ km}^2$ (11.5%) while grasslands and croplands retreated by $490,644 \text{ km}^2$ (4.6%) and $225,263 \text{ km}^2$ (1.2%) (Fig. 3d–f). Shrubs showed a 5-year increase after the 2002 drought and an overall increasing trend in shrublands (Fig. 3f), while grasses showed an initial 3-year increase after the 2002 drought then continuous decline afterward for 13 years (Fig. 3e).

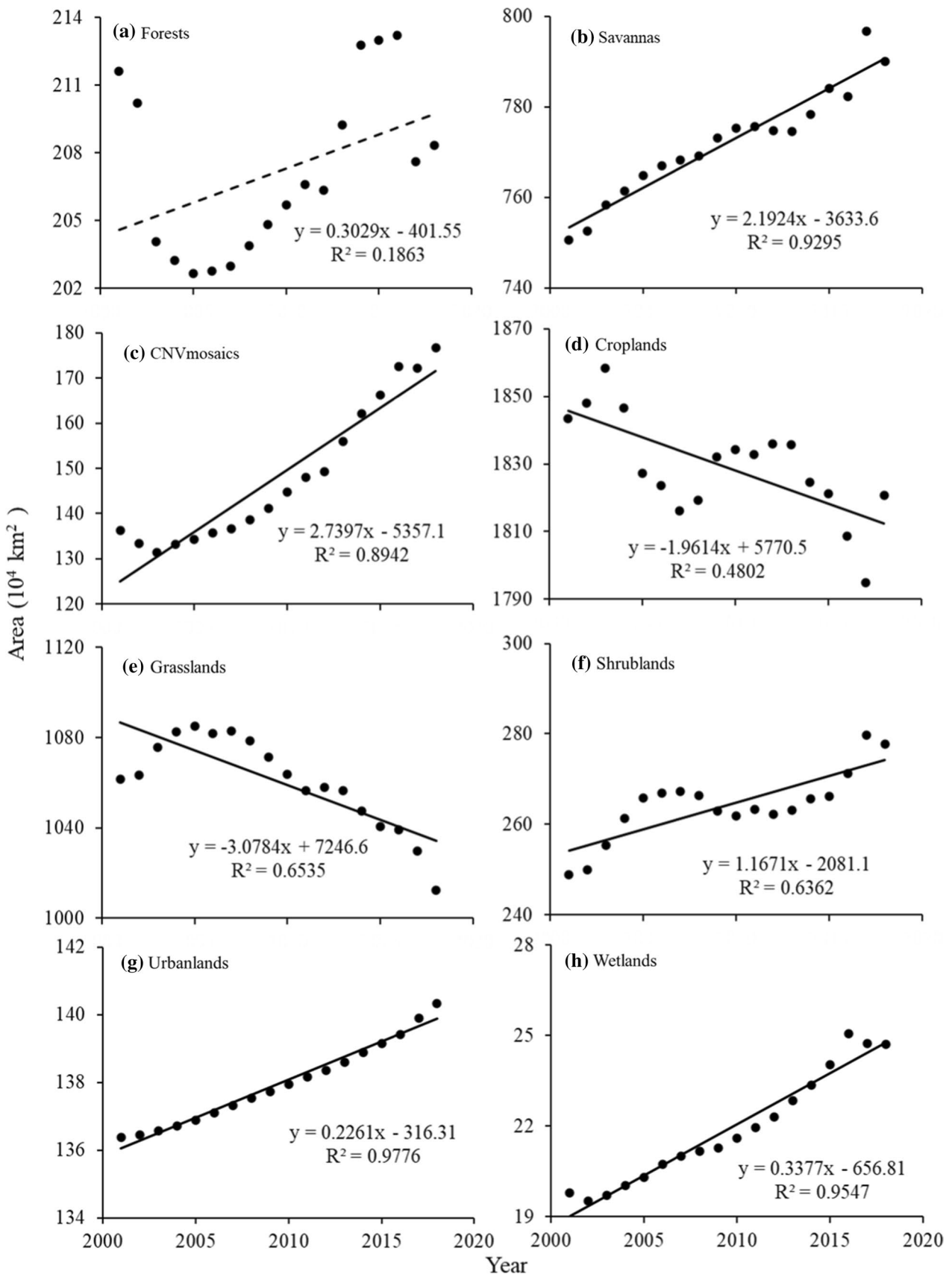


Fig. 3 Total area (km²) of eight vegetation types: **a**) forests, **b**) savannas, **c**) croplands, and natural vegetation (CNV) mosaics, **d**) croplands, **e**) grasslands, **f**) shrublands, **g**) urbanlands, and **h**) wetlands over the period of Jan. 1, 2001–Dec. 31, 2018 in Mediterranean Europe and North Africa (MENA, 20° W–45° E and 20° N–45° N)

Croplands occupied the largest area in 2003 (18,582,372 km²) both temporally across 18 years and spatially across eight vegetation types, right after the 2002 drought, then declined afterwards with fluctuations.

The area of permanent wetlands increased by 49,192 km² (24.9%), and that of urban land increased by 39,570 km² (2.9%) (Fig. 3g, h).

Matrices of landcover change

To quantify the direction and intensity of change, we used the area of each vegetation type that had changed to make transition matrices. A transition matrix could illustrate the detailed vegetation transition during either a short-term period (i.e. during 2002–2003 right after the 2002 heatwave/drought) or a long-term period (i.e. during 2001–2018) (Table 3; Fig. 4).

In Table 3, the diagonal cell areas remained in the same vegetation types. The upper right triangle portion indicates transitions to a less productive vegetation type, while the lower-left triangle indicates transitions to a more productive vegetation type, based on what we have learned from PDF curves of LAI and GPP deficits.

During 2002–2003, 17,775 km² of the forested area became less productive and remote sensing identified them as savannas, while a total of 22,680 km² of barren land became vegetated (turned into grassland and shrubland). As a result, a total of 52,986 km² became less productive based on the four categories with over 5000 km² (i.e. from forest to savanna, from savanna to grassland, from cropland to grassland, and from grassland to shrubland) while a total of 56,814 km² became more productive based the five categories listed in the lower triangle (i.e. from grassland to savanna, from grassland to cropland, from shrubland to grassland, and from barren land to either grassland or shrubland).

During 2001–2018, 55,948 km² of the forested area became less productive savannas (Fig. 4, visible in southern France and western Portugal) while 54,475 km² of savannas had the reversed transition, leaving a net loss of forests by a mere 1473 km². A total of 85,257 km² of barren land became vegetated (mostly turned into grassland and shrubland) and 27,609 km² of vegetated pixels became barren, leaving a net gain of 57,649 km² of the vegetated area from barren land (0.9%). Such green-up is visible in parts of northern Algeria and Tunisia, eastern Iran, northern Saudi Arabia and

northern Egypt (Fig. 4). There was a total area of 413,922 km² that became more productive and 260,560 km² became less productive (based only on categories of transition with 20,000 km² or more).

Discussion

One of the most climate sensitive regions of the world is the Mediterranean basin (MENA) (IPCC 2013). Changes in human population distribution, conflict, land management and land use have occurred concurrent with changes in climate and have altered vegetation patterns across the region, with feedback to the regional climate (Tanrivermis 2003; Serra et al. 2008; Bajocco et al. 2012; Millán 2014; Luysaert et al. 2014; Perugini et al. 2017; World Bank 2021; Wolpert et al. 2020; Ruiz and Sanz-Sánchez 2020). We recognize that in evaluating causes of regional vegetational changes it may be difficult to separate those induced by climate regionally from other causes of landscape-scale changes such as political and economic changes, particularly in regions of the globe that lack extensive data on land use and management, and considering the interactions of these societal factors with climate change is an important goal for future analyses, although difficult to do at this large spatial scale. Well-known examples of land use and management change not directly driven by climate in the MENA region include afforestation in Israel (Rotenberg and Yakir 2011), marsh drainage in southern Iraq (Hashim et al. 2019), irrigation intensification in several countries (Krakauer et al. 2020), and widespread urbanization (Rozalis et al. 2010). This report, however, is focused particularly on those potential causes that can be evaluated by satellite remote sensing and climate data and operate with some consistency across political boundaries, with an eye toward evaluating sub-continental to global-scale changes elsewhere in the world for which these data are readily available, while more fine-scale ground-based observational data (e.g. land use and management) are more difficult to retrieve. While policy and management can have an impact on local scale and stepwise changes, regional scale change in a long-term, which is our focus, should be dominated by climatic changes.

The aim of the study was to use LAI and GPP deficits to identify and better understand the impacts of the climate on landcover in the MENA region during 2001–2018. Specifically, we would like to 1) determine critical climate drivers for the variability of the landcover as a whole and several ecosystem types individually, 2) explore landcover-specific signatures over the span of climate conditions, and 3) identify landcover changes over time and relate these changes to climate changes (and other non-climatic drivers).

Table 2 Means and standard deviations (SD) of vegetation responses (i.e. annual Leaf Area Index (LAI) deficit and gross primary productivity (GPP, in $\text{g C m}^{-2} \text{ year}^{-1}$) deficit), climate conditions (i.e. annual mean temperature ($^{\circ}\text{C}$), precipitation (mm month^{-1}), temperature–precipitation (TP) index, dryness index, Standardized Precipitation Evapotranspiration Index (SPEI)), and area ($100,000 \text{ km}^2$) for each landcover type that remained as the same landcover type over 19 years (pixels at 500 m resolution)

	Years (n)	Forests		Savannas		CNV mosaic		Grasslands		Croplands		Shrublands		Wetlands		Urban	
		Mean	SD	Mean	SD	Mean	SD	Mean	SD	Mean	SD	Mean	SD	Mean	SD	Mean	SD
LAI deficit	19	135.3	13.4	85.04	8.85	81.73	7.11	39.66	4.61	80.97	6.00	17.70	2.48	72.57	6.18	47.22	3.69
GPP deficit ($\text{gC m}^{-2} \text{ year}^{-1}$)	19	1689	215.3	1489.04	199.604	1415	184.6	955.8	126.6	1414	167.4	509.1	66.47	1141	141.4	1082	131.0
Temperature ($^{\circ}\text{C}$)	19	10.00	0.47	12.04	0.37	12.26	0.38	11.46	0.48	13.60	0.36	17.46	0.32	14.74	0.36	14.23	0.37
Precipitation (mm month^{-1})	19	91.86	7.28	84.01	7.36	74.72	6.89	62.34	4.14	53.58	4.21	28.52	4.10	61.38	5.51	61.40	5.10
TP index	19	0.51	0.03	0.41	0.02	0.39	0.02	0.45	0.03	0.35	0.02	0.19	0.01	0.31	0.01	0.34	0.02
Dryness index	19	1.00	0.25	2.26	0.46	0.84	0.12	6.14	1.52	5.43	0.81	11.11	1.83	6.22	1.27	5.09	0.67
SPEI	19	-0.34	0.61	-0.45	0.52	-0.42	0.60	-0.31	0.47	-0.47	0.42	-0.64	0.62	-0.49	0.49	-0.51	0.41
Area ($100,000 \text{ km}^2$)	18	20.72	0.37	77.21	1.21	14.83	1.55	106.04	2.03	182.91	1.51	26.42	0.78	2.19	0.18	13.80	0.12

Vegetation-centric approach of LAI and GPP deficits

LAI and GPP deficits provide a different perspective into the climate-vegetation interaction, in contrast to the traditional climate anomaly approach.

Through examining the responses of LAI deficit and GPP deficit of all vegetation types combined and individually to various climate indices including T , P , TP Index, dryness and SPEI, both LAI and GPP deficits proved to be effective indicators of how ecosystem photosynthetic structures and functions respond to climate stress. This study took this as a starting point to further explore the responses of the two deficits to interannual variations of the climatic conditions for the MENA region.

The perfect-deficit approach was used at a monthly scale derived from the original 16-day product, which is much less sensitive to extreme value than a daily or hourly product. Technical documentation of MODIS LAI and GPP products listed detailed uncertainty evaluation rules. The MODIS LAI/FPAR algorithm consists of a main look-up-table (LUT) based procedure (Knyazikhin et al. 1998) that exploits the spectral information content of the MODIS red (648 nm) and near-infrared (NIR 858 nm) surface reflectance, and the backup algorithm that uses empirical relationships between Normalized Difference Vegetation Index (NDVI) and canopy LAI and FPAR. The theoretical estimates of uncertainties (%) in the BRFs used in the C6 LAI/FPAR algorithm are 20–30% for red and 5–15% for NIR. The validation strategy for MODIS GPP was initially established based on Running et al. (1999) and has been widely accepted and applied in numerous publications (e.g. Turner et al. 2003, 2004, 2006).

In general, regressions of LAI deficits and GPP deficits behaved very similarly, except to precipitation (Fig. 2c, d). Both Forest and overall LAI deficits ($\text{m}^2 \text{ m}^{-2}$) had a positive correlation with annual precipitation (mm), which was quite counter-intuitive. To understand this, we can start with Fig. 2d.

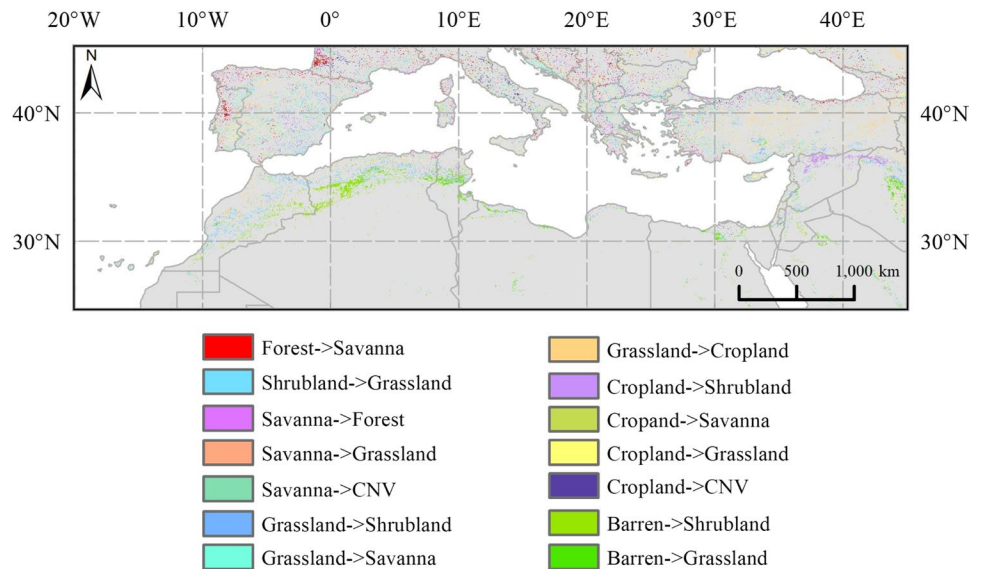
Within each vegetation type, GPP deficits (kg C m^{-2}) decreased when annual precipitation (mm) increased, which meant less GPP loss within the same year with more precipitation. This is consistent with existing literature (Wu et al. 2011; Nielsen and Ball 2015). The overall regression of GPP deficits over precipitation, however, had a counter-intuitively positive slope, which was overwhelmingly dominated by intrinsic variation among different vegetation types (i.e. forests generally have the highest GPP base. Therefore, its absolute increase in response to increasing precipitation should be the highest). The overall pattern was more strongly driven by intrinsic productivities of each vegetation type rather than local responses to climate variables alone.

Likely, as in Fig. 2c, the overall regression of LAI deficits over precipitation had a positive slope, with the same reason as for GPP deficits—they are tightly constrained within

Table 3 Areas (km²) of major vegetation type transition from 2002 (in rows) to 2003 (in columns (categories > 5000 km²) and from 2001 to 2018 (categories with > 20,000 km²), with the italicized diagonal cells being areas remained in the same landcover types

Area (km ²) of vegetation transition	Forest	Savanna	CNV mosaic	Cropland	Wetland	Urban	Grassland	Shrubland	Barren	Water
2002\2003 (only categories with > 5000 km ² were listed)										
Forest	539,687	17,775								
Savanna	(3854)	845,142					17,186			
CNV mosaic			89,324							
Cropland				1,518,885			10,727			
Wetland					16,949					
Urban						104,781				
Grassland		9834		15,729			1,025,717	7298		
Shrubland							8570	343,054		
Barren							9879	12,801	6,367,401	
Water										11,527,805
2001\2018 (only categories with > 20,000 km ² were listed)										
Forest	500,508	55,948								
Savanna	54,475	716,599	21,938				57,586			
CNV mosaic			71,082							
Cropland		22,846	29,875	1,390,808			63,253	22,897		
Wetland					14,708					
Urban						104,735				
Grassland		106,902		77,943			814,238	38,938		
Shrubland							37,853	280,748		
Barren							31,652	52,376	6,309,837	
Water										11,525,705

Fig. 4 Map showing changes of landcover types during 2001–2018 (500 m resolution) in Mediterranean Europe and North Africa (MENA, 20° W–45° E and 20° N–45° N)



each vegetation type. However, within forests, the regression slope was also positive. To understand this pattern, we should also look at what has happened to the area (Fig. 3a; Table 3). In 2002, the MENA region experienced a widespread severe drought. The total area of forests decreased

drastically from 2,102,011 km² in 2002 to 2,040,610 km² in 2003, and it continued to decline for two more years that followed, with 2005 having the smallest area of forests. It took another 10 years (2005–2014) for the area of forests to restore to the pre-drought level. In other words, there were

3 years of lag and 10 years of legacy effects in terms of the distribution area of forests. Similarly, forest area was at its highest in 2017, then declined drastically in 2018, possibly due to another extreme event.

If we looked at the time series of LAI deficits, similar lag and legacy effects existed. The decline of LAI happened in the following few years, therefore, LAI was at its highest when precipitation was at its lowest, or LAI deficit was the lowest when climate conditions (such as precipitation) suddenly became less optimal. Therefore, we see this counter-intuitive positive slope for regression of LAI deficits over annual precipitation.

Five climate indices

There are many climate indices available. For this study, we used two primary instrumental measures (temperature and precipitation) and three compound climate indices, each presenting a different group of indices that emphasize certain aspects of hydro and/or thermal conditions. Dryness index is expressed in a linear relationship between net radiation and precipitation; TP index is expressed with an exponential formula, containing temperature and precipitation; SPEI is a standardized index allowing flexibility of temporal scales.

Because Dryness, TP index, and SPEI all contain the information of precipitation and are not independent of each other, multiple univariate regressions might be easier to interpret than a single multivariate regression.

When response variables LAI deficit and GPP deficit were plotted against each of the five climate indices, all except SPEI were tightly clustered within each vegetation type (Fig. 2; Table 2). Because SPEI is a standardized index, site specificity has been removed during the calculation. On the other hand, these tightly distributed clusters may indicate strong resistance to transitions between vegetation types and alternative stable states caused by the changing climate (Hirota et al. 2011; Chapin et al. 2011). Although they currently seem to be within the resilience ranges, further studies with finer spatial and temporal scales, and with a finer categorization of vegetation types and functional groups could tell a different story. Patterns operating at finer scales will be different from what has been looked at (bigger scales), but this may not necessarily lead to a better understanding of the processes operating at the coarser resolution we have studied (Liao et al. 2020; Chen 2021; Chen et al. 2021; Guo et al. 2021).

Eight vegetation covers and their PDFs

Despite their structural and functional responses to climate and ecological conditions, most vegetation types are tightly constrained, representing steady states for specific combinations of climate conditions and their immediate alternative

steady states if strong enough forces change them one way or another (Fig. 2).

Opposite to patterns in the forests, shrubland LAI deficit was positively correlated with dryness index. However, that does not necessarily mean if the area experienced prolonged directional change related to temperature, water availability and solar radiation, a transition of vegetation coverage between forests and shrubland could happen. When we looked deeply into the ranges of annual average temperature (10.0 ± 0.5 vs 17.5 ± 0.3 °C), precipitation (91.86 ± 7.28 vs 28.52 ± 4.1 mm month⁻¹), TP index (0.51 ± 0.03 vs 0.19 ± 0.01), Dryness (1.00 ± 0.25 vs 11.11 ± 1.83), and SPEI (-0.34 ± 0.61 vs -0.64 ± 0.62) of forest and shrubland (Table 1), forest, and shrubland are experiencing very different local climate changes, thus leading to polar opposite responses. The results are consistent with the “16 °C threshold” prediction (Yi et al. 2010), which stated that the exchanges of carbon, water, and energy between terrestrial ecosystems and the atmosphere are limited primarily by water availability when the mean annual temperature is above a threshold of 16 °C and by temperature when below 16 °C. Other studies also have looked into the changes in landcover under the influence of climate change. For example, Vidal-Macua et al. (2017) studied factors affecting forest dynamics in the Iberian Peninsula from 1987 to 2012 based on Landsat scenes, and found that the geographical transition from shrubland to forests is closely related to higher soil moisture (Topographic Wetness Index—TWI) and lower winter solar radiation. Meanwhile, strategies aiming at decreasing the risk of decline and promoting resistance to abrupt stress in the short term may not enhance long-term resilience (Vilà-Cabrera et al. 2018).

Landcover changes and their implications

Combining with transition maps, the transition matrix is a powerful tool to specify the direction and intensity of landscape changes over the region. Comparing short-term and long-term transition matrices can also indicate how vegetation responds to extreme events (such as the 2002 drought) immediately and in a long run.

Even though the percentage of vegetated area of forest (4.7%) was far less than cropland (41.2%), grassland (23.9%), savanna (17.4%), and shrubland (6.0%), the patterns of LAI deficit of forest were always consistent with the LAI and GPP deficit of all vegetation types, which indicates the strong forest LAI response to climate and its dominating influence over the response of the integrated vegetated landcover in our analysis. The MENA area was still benefiting from the increase of ambient temperature and CO₂ during 2001–2018, as indicated by the green-up of barren land and the gradual recovery of forested areas after the 2002 drought. Vegetation response to elevated CO₂ is conserved

across a broad range of productivity (Norby et al. 2005), but what was initially observed in the temperate free-air CO₂ enrichment (FACE) experiments (Hendrey 1992; Hendrey et al. 1999) may not be representative of other regions (Hickler et al. 2008), particularly in degrading landscapes, and belowground response could be more continuous than aboveground response to CO₂ enrichment (Jackson et al. 2009) which cannot be detected by satellite data.

This analysis of available data indicates that overall, forests, cropland, and grassland are more vulnerable to climate stress, thus declining over the past 18 years, while savanna and shrubland are more resilient and their distribution expanded. Expansion of shrubland seems to be counter to the need for improved agriculture and forestry goals of land managers (World Bank 2021), supporting our thesis that climate change is a key driver of the trends described here.

The two dominant vegetated landcovers in this area, cropland (41.2%) and grassland (23.9%) (Table 2), fluctuated in opposite patterns over the years (Fig. 3). This is likely due to the expansion of cropland that was usually an encroachment into grassland, while fallow croplands generally returned to grassland.

One of the most striking patterns was the areas of increased shrubs that replaced cropland and grasses (upstream of productivity) and barren land (downstream of productivity). According to the areal changes of vegetation covers during 2001–2018 (partly in Table 3b), a total area of 38,938 km² was converted from grassland to shrubland and 22,897 km² from cropland to shrubland. At the same time, 37,853 km² of shrubland was converted back to grassland and 14,163 km² back to cropland, perhaps as a result of improved land management. Further, a total area of 52,376 km² was converted from barren land to shrubland, while 15,232 km² of shrubland were converted back to barren land, and neither of these directional changes would seem to be a desirable outcome for current land management practices (World Bank 2021). There have been various reports on local shrubland dieback in south Spain (Lloret et al. 2016) and the overall trend of shrubland cover based on satellite data for the entire MENA region shows increasing dieback.

With higher temperature and more extended period of drought, MENA is becoming less productive (with fewer forests and croplands) with more shrubby vegetation covers, with just a small fraction of barren land (less than 1%) that became vegetated. Although some authors (e.g. Bastin et al. 2019) have recently advocated for tree plantation to combat desertification derived from global change, our study suggests that a more resilient (and short) vegetation might be more suitable for restoration programs in areas like MENA.

The central location and average altitude of forest vegetation have not yet changed despite the changes in temperature and dryness. On the other hand, the mean and median latitude of cropland decreased over the last decade, likely due to

human effort in improving irrigation systems for agriculture purposes. The mean latitude and median elevation of grassland also decreased over the last decade. Any increase in grassland probably benefited from the fertilization effect of elevated ambient CO₂ concentration. This also might have a tight association with the escalating incidence of wildfire near arid and semiarid areas throughout the world, some of which have caused devastating losses (Bladon 2018; Bowman et al. 2020; European Commission 2021).

For 2001–2018, the mean latitude ($R^2=0.864$, $p<0.001$) and median latitude ($R^2=0.513$, $p<0.05$) of cropland both decreased significantly. Such a counter-intuitive change is probably due to the huge effort of human intervention: establishing irrigation systems and building dams for agriculture (United Nations 1999; FAO 2008).

The mean latitude ($R^2=0.779$, $p<0.001$) and median elevation ($R^2=0.473$, $p<0.05$) of grassland also decreased significantly. Prior field manipulation experiments have shown that elevated ambient CO₂ concentration can stimulate the growth and accumulation of standing biomass of grassland in semiarid areas, acting like a carbon fertilizer and a booster of water use efficiency (Dijkstra et al. 2010). Grasses dieback during the dry seasons, which naturally turn into standing fuel, causing increasing wildfire risk and devastating loss. This has been happening throughout the world, especially in Mediterranean ecoregions such as California, US (Abatzoglou and Williams 2016; Parks et al. 2017; Goss et al. 2020).

The area of permanent wetlands increased by 49,192 km² (24.9%) most likely due to sea level rise. At the same time, urban land also increased by 39,570 km² (2.9%) (Fig. 3g, h), which reflects the urbanization in the region.

Conclusions

- LAI and GPP deficits, the vegetation-centric approach, provide a useful means to differentiate structural and function responses among different vegetation types under climate stress in the MENA regions, showing the areas and productivities of different vegetation types have experienced significant short-term and long-term changes in response to varying climate and non-climatic (e.g. land management) conditions during 2001–2019.
- Over the study period, the areas of savannas and CNV mosaics increased by 394,994 km² and 404,592 km², respectively, while that of forests decreased by 33,091 km². Meanwhile, shrublands extended by 287,134 km² while grasslands and croplands retreated by 490,644 km² and 225,263 km², respectively. The area of wetlands increased by 49,192 km², and that of urban land increased by 39,570 km². Finally, 57,649 km² of barren land became vegetated over the years.

- Vegetation responses to climate variations depend on vegetation types with distinctive yet overlapping signatures over the span of climate conditions considered. The climate sensitivity decreases in the following order: forests, savannas, a mosaic of cropland and natural vegetation (CNV), croplands, permanent wetlands, urban land, grasslands, and shrublands. Shrubs were the most resilient under a hotter and drier climate. Forests showed the strongest and most dominating response to severe drought with a lag of 1–3 years and a legacy effect for 10 years.

Supplementary Information The online version contains supplementary material available at <https://doi.org/10.1007/s00442-021-05041-3>.

Acknowledgements We thank anonymous reviewers for their helpful and constructive comments that improved previous versions of the manuscript. This manuscript is to be published as part of a Special Issue honoring Russ Monson. We appreciate particularly Russ' academic leadership and contributions to plant evolution, plant ecology, and ecosystem ecology.

Author contribution statement CY designed the research with WF. WF performed analysis with CY. WF processed the data with KJ, ZL, PX, and SG. WF drafted the first manuscript and DC substantially improved the interpretation of results. All authors discussed the results and contributed to the final manuscript.

Funding We acknowledge the funding support of the NSF 81620108010 for WF, PSC-CUNY ENHC-48-33 and CUNY CIRG-80209-08 22 for CY, Natural Science Foundation of Anhui province of China (NO. 2008085QD167) for PX, and Federal Work-Study Undergraduate Research Assistantship for GL.

Availability of data and code The datasets and code used and/or analyzed during the current study are available from the corresponding author on reasonable request.

Declarations

Conflict of interest The authors declare that they have no conflict of interest.

Ethical approval This article does not contain any studies with human participants or animals performed by any of the authors.

References

- Abatzoglou JT, Williams AP (2016) Impact of anthropogenic climate change on wildfire across western US forests. *Proc National Acad Sci* 113(42):11770–11775. <https://doi.org/10.1073/pnas.1607171113>
- Alexandrian D, Esnault F, Calabri G (1998) Forest fires in the Mediterranean area. In: <http://www.fao.org/3/x1880e/x1880e07.htm>. Accessed 21 June 2021
- Allen CD, Macalady AK, Chenchouni H, Bachelet D, McDowell N, Vennetier M (2010) A global overview of drought and heat-induced tree mortality reveals emerging climate change risks for forests. *For Ecol Manag* 259(4):660–684. <https://doi.org/10.1016/j.foreco.2009.09.001>
- Allen CD, Breshears DD, McDowell NG (2015) On underestimation of global vulnerability to tree mortality and forest die-off from hotter drought in the Anthropocene. *Ecosphere* 6(8):1–55. <https://doi.org/10.1890/ES15-00203.1>
- Anderegg WRL, Kane JM, Anderegg LDL (2012) Consequences of widespread tree mortality triggered by drought and temperature stress. *Nat Clim Change* 3:30–36. <https://doi.org/10.1038/nclimate1635>
- Assal TJ, Anderson PJ, Sibold J (2016) Spatial and temporal trends of drought effects in a heterogeneous semi-arid forest ecosystem. *For Ecol Manag* 365:137–151. <https://doi.org/10.1016/j.foreco.2016.01.017>
- Bajocco S, Angelis AD, Perini L, Ferrara A, Salvati L (2012) The impact of land use/land cover changes on land degradation dynamics: a Mediterranean case study. *Environ Manag* 49(5):980–989. <https://doi.org/10.1007/s00267-012-9831-8>
- Bastin JF, Finegold Y, Garcia C, Mollicone D, Rezende M, Routh D (2019) The global tree restoration potential. *Science* 365(6448):76–79. <https://doi.org/10.1126/science.aax0848>
- Bladon KD (2018) Rethinking wildfires and forest watersheds. *Science* 359(6379):1001–1002. <https://doi.org/10.1080/00385417.1961.10770761>
- Bowman DMJS, Kolden CA, Abatzoglou JT, Johnston FH, van der Werf GR, Flannigan M (2020) Vegetation fires in the Anthropocene. *Nat Rev Earth Environ* 1:500–515. <https://doi.org/10.1073/pnas.1010070108>
- Budyko MI (1961) The heat balance of the Earth's surface. *Sov Geogr* 2:3–13. <https://doi.org/10.1080/00385417.1961.10770761>
- Carnicer J, Coll M, Ninyerola M, Pons X, Sánchez G, Peñuelas J (2011) Widespread crown condition decline, food web disruption, and amplified tree mortality with increased climate change-type drought. *PNAS* 108:1474–1478. <https://doi.org/10.1073/pnas.1010070108>
- Chapin FS, Matson PA, Vitousek PM (2011) Temporal dynamics. In: *Principles of terrestrial ecosystem ecology*, 2nd edn. Pp 339–367
- Chen D (2021) Impact of climate change on sensitive marine and extreme terrestrial ecosystems: recent progresses and future challenges. *Ambio* 50:1141–1144. <https://doi.org/10.1007/s13280-020-01446-1>
- Chen Z, Liu H, Xu C, Wu X, Liang B, Cao J, Chen D (2021) Modeling vegetation greenness and its climate sensitivity with deep-learning technology. *Ecol Evol* 11:7335–7345. <https://doi.org/10.1002/ece3.7564>
- Ciais P, Reichstein M, Viovy N, Grainer A, Ogee J, Allard V (2005) Europe-wide reduction in primary productivity caused by the heat and drought in 2003. *Nature* 437(7058):529–533. <https://doi.org/10.1038/nature03972>
- Cramer W, Guiot J, Fader M, Garrabou J, Gattuso JP, Iglesias A, Xoplaki E (2018) Climate change and interconnected risks to sustainable development in the Mediterranean. *Nat Clim Change* 8(11):972–980. <https://doi.org/10.1038/s41558-018-0299-2>
- Dijkstra FA, Blumenthal D, Morgan JA, LeCain DR, Follett RF (2010) Elevated CO₂ effects on semi-arid grassland plants in relation to water availability and competition. *Funct Ecol* 24:1152–1161. <https://doi.org/10.1111/j.1365-2435.2010.01717.x>
- European Commission (2021) Energy, climate change, environment. https://ec.europa.eu/info/energy-climate-change-environment_en
- Fischer EM, Knutti R (2015) Anthropogenic contribution to global occurrence of heavy-precipitation and high-temperature extremes.

- Nat Clim Change 5(6):560–564. <https://doi.org/10.1038/nclimate2617>
- Food and Agriculture Organization (2008) The near East and North Africa: growing demand, limited resources. FAO Newsroom. Accessed 21 June 2021
- Foley JA, Prentice IC, Ramankutty N, Levis S, Pollard D, Sitch S (1996) An integrated biosphere model of land surface processes, terrestrial carbon balance, and vegetation dynamics. *Glob Biogeochem Cycles* 10:603–628. <https://doi.org/10.1029/96GB02692>
- Friend AD (2010) Terrestrial plant production and climate change. *J Exp Bot* 61:1293–1309. <https://doi.org/10.1093/jxb/erq019>
- Goss M, Swain DL, Abatzoglou JT, Sarhadi A, Kolden CA, Williams AP (2020) Climate change is increasing the likelihood of extreme autumn wildfire conditions across California. *Environ Res Lett* 15:094016. <https://doi.org/10.1088/1748-9326/ab83a7>
- Guo L, Li T, Chen D, Liu J, He B, Zhang Y (2021) Links between global terrestrial water storage and large-scale modes of climatic variability. *J Hydrol* 598:126419. <https://doi.org/10.1016/j.jhydrol.2021.126419>
- Hashim BM, Sultan MA, Attyia MN, Al Maliki AA, Al-Ansari N (2019) Change detection and impact of climate changes to Iraqi southern marshes using Landsat 2 MSS, Landsat 8 OLI and Sentinel 2 MSI data and GIS applications. *Appl Sci* 9(10):2016. <https://doi.org/10.3390/app9102016>
- Hendrey GR (1992) FACE: free-air CO₂ enrichment for plant research in the field. Introduction. *Crit Rev Plant Sci* 11:59–60. <https://doi.org/10.1080/07352689209382330>
- Hendrey GR, Ellsworth DS, Lewin KF, Nagy J (1999) A free-air enrichment system for exposing tall forest vegetation to elevated atmospheric CO₂. *Glob Change Biol* 5:293–309. <https://doi.org/10.1046/j.1365-2486.1999.00228.x>
- Hickler T, Smith B, Prentice IC, Mjöfors K, Miller P, Arneth A (2008) CO₂ fertilization in temperate FACE experiments not representative of boreal and tropical forests. *Glob Change Biol* 14:1531–1542. <https://doi.org/10.1111/j.1365-2486.2008.01598.x>
- Hirota M, Holmgren M, Nes EHV, Scheffer M (2011) Global resilience of tropical forest and Savanna to critical transitions. *Science* 334:232–235. <https://doi.org/10.1126/science.1210657>
- Huang K, Yi C, Wu D, Zhou T, Zhao X, Blanford W (2015) Tipping point of a conifer forest ecosystem under severe drought. *Environ Res Lett* 10:024011. <https://doi.org/10.1088/1748-9326/10/2/024011>
- IPCC (2013) Climate change 2013: the physical science basis. Contribution of Working Group I to the fifth assessment report of the intergovernmental panel on climate change. Cambridge University Press, Cambridge, p 153. <https://doi.org/10.1017/CBO9781107415324>
- Jackson RB, Cook CW, Phippen JS, Palmer SM (2009) Increased below-ground biomass and soil CO₂ fluxes after a decade of carbon dioxide enrichment in a warm-temperate forest. *Ecology* 90:3352–3366. <https://doi.org/10.1890/08-1609.1>
- Jenny H (1984) The soil resource. Origin and behavior. *Vegetation* 57:102–102. <https://doi.org/10.1007/BF00047304>
- Jump AS, Peñuelas J (2005) Running to stand still: adaptation and the response of plants to rapid climate change. *Ecol Lett* 8:1010–1020. <https://doi.org/10.1111/j.1461-0248.2005.00796.x>
- Kerr JT, Ostrovsky M (2003) From space to species: ecological applications for remote sensing. *Trends Ecol Evol* 18:299–305. [https://doi.org/10.1016/S0169-5347\(03\)00071-5](https://doi.org/10.1016/S0169-5347(03)00071-5)
- Knyazikhin Y, Martonchik JV, Myneni RB, Diner DJ, Running SW (1998) Synergistic algorithm for estimating vegetation canopy leaf area index and fraction of absorbed photosynthetically active radiation from MODIS and MISR data. *J Geophys Res Atmos* 103:32257–32275. <https://doi.org/10.1029/98JD02462>
- Krakauer NY, Cook BI, Puma MJ (2020) Effect of irrigation on humid heat extremes. *Environ Res Lett* 15(9):094010. <https://doi.org/10.1088/1748-9326/ab9ecf>
- Liang S (2018) Remote sensing of earth’s energy budget: an overview of recent progress. In: *Comprehensive remote sensing, earth’s energy budget*, vol 5, pp 1–31. <https://doi.org/10.1016/B978-0-12-409548-9.10365-3>
- Liao C, Qiu J, Chen B, Chen D, Fu B, Wu J (2020) Advancing landscape sustainability science: theoretical foundation and synergies with innovations in methodology, design, and application. *Landsc Ecol* 35:1–9. <https://doi.org/10.1007/s10980-020-00967-0>
- Lloret F, Riva EGD, Pérez-Ramos IM, Marañón T, Saura-Mas S, Díaz-Delgado R (2016) Climatic events inducing die-off in Mediterranean shrublands: are species’ responses related to their functional traits? *Oecologia* 180:961–973. <https://doi.org/10.1007/s00442-016-3550-4>
- Luysaert S, Jammert M, Stoy P (2014) Land management and land-cover change have impacts of similar magnitude on surface temperature. *Nat Clim Change* 4:389–393. <https://doi.org/10.1038/nclimate2196>
- Martínez-Vilalta J, Piñol J, (2002) Drought-induced mortality and hydraulic architecture in pine populations of the NE Iberian Peninsula. *For Ecol Manag* 161:247–256. [https://doi.org/10.1016/S0378-1127\(01\)00495-9](https://doi.org/10.1016/S0378-1127(01)00495-9)
- Matusick G, Ruthrof KX, Brouwers NC, Dell B, Hardy G (2013) Sudden forest canopy collapse corresponding with extreme drought and heat in a Mediterranean-type eucalypt forest in Southwestern Australia. *Eur J for Res* 132:497–510. <https://doi.org/10.1007/s10342-013-0690-5>
- McNally A, Arsenault K, Kumar S, Shukla S, Peterson P, Wang S, Verdin JP (2017) A land data assimilation system for sub-Saharan Africa food and water security applications. *Sci Data* 4(1):1–19. <https://doi.org/10.1038/sdata.2017.12>
- Millán MM (2014) Extreme hydrometeorological events and climate change predictions in Europe. *J Hydrol* 518:206–224. <https://doi.org/10.1016/j.jhydrol.2013.12.041>
- Myneni RB, Maggion S, Iaquinta J, Privette JL, Gorbun N, Pinty B (1995a) Optical remote sensing of vegetation: modeling, caveats, and algorithms. *Remote Sens Environ* 51:169–188. [https://doi.org/10.1016/0034-4257\(94\)00073-V](https://doi.org/10.1016/0034-4257(94)00073-V)
- Myneni RB, Hall FG, Sellers PJ, Marshak AL (1995b) The interpretation of spectral vegetation indexes. *IEEE Trans Geosci Remote Sens* 33:481–486. <https://doi.org/10.1109/36.377948>
- Nielsen UN, Ball BA (2015) Impacts of altered precipitation regimes on soil communities and biogeochemistry in arid and semi-arid ecosystems. *Glob Change Biol* 21:1407–1421. <https://doi.org/10.1111/gcb.12789>
- Norby RJ, Delucia EH, Gielen B, Calfapietra C, Giardina C, King J, Oren R (2005) Forest response to elevated CO₂ is conserved across a broad range of productivity. *Proc Natl Acad Sci* 102:18052–18056. <https://doi.org/10.1073/pnas.0509478102>
- Parks SA, Holsinger LM, Miller C, Parisien MA (2017) Analog-based fire regime and vegetation shifts in mountainous regions of the western US. *Ecography* 41:910–921. <https://doi.org/10.1111/ecog.03378>
- Peñuelas J, Sardans J (2021) Global change and forest disturbances in the mediterranean basin: breakthroughs knowledge gaps and recommendations. *Forests* 12(5):603. <https://doi.org/10.3390/f12050603>
- Peñuelas J, Lloret F, Montoya R (2001) Severe drought effects on Mediterranean woody flora in Spain. *For Sci* 47(2):214–218. [https://doi.org/10.1016/S0378-1127\(00\)00582-X](https://doi.org/10.1016/S0378-1127(00)00582-X)
- Perugini L, Caporaso L, Marconi S, Cescatti S, Quesada A, Arneth A (2017) Biophysical effects on temperature and precipitation due to land cover change. *Environ Res Lett*. <https://doi.org/10.1088/1748-9326/aa6b3f>

- Rotenberg E, Yakir D (2011) Distinct patterns of changes in surface energy budget associated with forestation in the semiarid region. *Glob Change Biol* 17:1536–1548. <https://doi.org/10.1111/j.1365-2486.2010.02320.x>
- Rozalis S, Morin E, Yair Y, Price C (2010) Flash flood prediction using an uncalibrated hydrological model and radar rainfall data in a Mediterranean watershed under changing hydrological conditions. *J Hydrol* 394(1–2):245–255. <https://doi.org/10.1016/j.jhydrol.2010.03.021>
- Ruiz I, Sanz-Sánchez MJ (2020) Effects of historical land-use change in the Mediterranean environment. *Sci Total Environ* 732:139315. <https://doi.org/10.1016/j.scitotenv.2020.139315>
- Running SW, Baldocchi DD, Turner DP, Gower ST, Bakwin PS, Hibbard KA (1999) A global terrestrial monitoring network integrating tower fluxes, flask sampling, ecosystem modeling and EOS satellite data. *Remote Sens Environ* 70(1):108–127. [https://doi.org/10.1016/S0034-4257\(99\)00061-9](https://doi.org/10.1016/S0034-4257(99)00061-9)
- Seguí PQ, Ribes A, Martín E, Habets F, Boé J (2010) Comparison of three downscaling methods in simulating the impact of climate change on the hydrology of Mediterranean basins. *J Hydrol* 383(1–2):111–124. <https://doi.org/10.1016/j.jhydrol.2009.09.050>
- Serra P, Pons X, Saurí D (2008a) Land-cover and land-use change in a Mediterranean landscape: a spatial analysis of driving forces integrating biophysical and human factors. *Appl Geogr* 28(3):189–209. <https://doi.org/10.1016/j.apgeog.2008.02.001>
- Serra P, Pons X, Saurí D (2008b) Land-cover and land-use change in a Mediterranean landscape: a spatial analysis of driving forces integrating biophysical and human factors. *Appl Geogr* 28:189–209. <https://doi.org/10.1016/j.apgeog.2008.02.001>
- Sitch S, Smith B, Prentice IC, Arneth A, Bondeau A, Sykes MT (2003) Evaluation of ecosystem dynamics, plant geography and terrestrial carbon cycling in the LPJ dynamic global vegetation model. *Glob Change Biol* 9:161–185. <https://doi.org/10.1046/j.13652486.2003.00569.x>
- Somot S, Sevault F, Déqué M, Crépon M (2008) 21st century climate change scenario for the Mediterranean using a coupled atmosphere–ocean regional climate model. *Glob Planet Change* 63:112–126. <https://doi.org/10.1016/j.gloplacha.2007.10.003>
- Sprintsin M, Karnieli A, Berliner P, Rotenberg E, Yakir D, Cohen S (2009) Evaluating the performance of the MODIS Leaf Area Index (LAI) product over a Mediterranean dryland planted forest. *Int J Remote Sens* 30(19):5061–5069. <https://doi.org/10.1080/01431160903032885>
- Tanrivermis H (2003) Agricultural land use change and sustainable use of land resources in the Mediterranean Region of Turkey. *J Arid Environ* 54(3):553–564. <https://doi.org/10.1006/jare.2002.1078>
- Turner DP, Urbanski S, Bremer D, Wofsy SC, Meyers T, Gregory M (2003) *Glob Change Biol* 9(3):383–395. <https://doi.org/10.1016/j.rse.2006.02.017>
- Turner DP, Ollinger S, Smith ML, Krankina O, Gregory M (2004) Scaling net primary production to a MODIS footprint in support of earth observing system product validation. *Int J Remote Sens* 25:1961–1979. <https://doi.org/10.1046/j.1365-2486.2003.00573.x>
- Turner DP, Ritts WD, Cohen WB, Gower ST, Running SW, Ahl DE (2006) Evaluation of MODIS NPP and GPP products across multiple biomes. *Remote Sens Environ* 102(3):282–292. <https://doi.org/10.1080/0143116031000150013>
- United Nations. Economic Commission for Africa. Subregional Office for North Africa (1999) Relevant water management and irrigation issues in North Africa. [Addis Ababa] © UN. ECA
- Vanacker V, Linderman M, Lupo F, Flasse S, Lambin E (2005) Impact of short-term rainfall fluctuation on interannual land cover change in sub-Saharan Africa. *Glob Ecol Biogeogr* 14:123–135. <https://doi.org/10.1111/j.1466-822X.2005.00136.x>
- Vicente-Serrano SM, Beguería S, López-Moreno JI (2010) A multi-scalar drought index sensitive to global warming: the standardized precipitation evapotranspiration index. *J Clim* 23:1696–1718. <https://doi.org/10.1175/2009JCLI2909.1>
- Vicente-Serrano SM, Beguería S, Lorenzo-Lacruz J, Camarero JJ, López-Moreno JI, Sanchez-Lorenzo A (2012a) Performance of drought indices for ecological, agricultural, and hydrological applications. *Earth Interact* 16:1–27. <https://doi.org/10.1175/2012EI000434.1>
- Vicente-Serrano S, Zouber A, Lasanta T, Pueyo Y (2012b) Dryness is accelerating degradation of vulnerable shrublands in semi-arid Mediterranean environments. *Ecol Monogr* 82(4):407–428. <https://doi.org/10.1890/11-2164.1>
- Vidal-Macua JJ, Ninyerola M, Zabala A, Domingo-Marimon C, Pons X (2017) Factors affecting forest dynamics in the Iberian Peninsula from 1987 to 2012. The role of topography and drought. *For Ecol Manag* 406:290–306. <https://doi.org/10.1016/j.foreco.2017.10.011>
- Vilà-Cabrera A, Coll L, Martínez-Vilalta J, Retana J (2018) Forest management for adaptation to climate change in the Mediterranean basin: a synthesis of evidence. *For Ecol Manag* 407:16–22. <https://doi.org/10.1016/j.foreco.2017.10.021>
- Wolpert F, Quintas-Soriano C, Plieninger T (2020) Exploring land-use histories of tree-crop landscapes: a cross-site comparison in the Mediterranean basin. *Sustain Sci* 15:1267–1283. <https://doi.org/10.1007/s11625-020-00806-w>
- World Bank (2021) Climate change knowledge portal. <https://climateknowledgeportal.worldbank.org/>
- Wu Z, Dijkstra P, Koch GW, Peñuelas J, Hungate BA (2011) Responses of terrestrial ecosystems to temperature and precipitation change: a meta-analysis of experimental manipulation. *Glob Change Biol* 17:927–942. <https://doi.org/10.1111/j.1365-2486.2010.02302.x>
- Yi C, Lui KY, Li TJ (1996) Research on relations of soil zonal distributions with climate in the monsoon region of the eastern part of China. *Acta Pedol Sin* 32:385–390
- Yi C, Ricciuto D, Li R, Wolbeck J, Xu X, Arain MA (2010) Climate control of terrestrial carbon exchange across biomes and continents. *Environ Res Lett* 5(3):034007. <https://doi.org/10.1088/1748-9326/5/3/034007>
- Yi C, Rustic G, Xu X, Wang J, Dookie A, Wei S (2012) Climate extremes and grassland potential productivity. *Environ Res Lett* 7(3):035703. <https://doi.org/10.1088/1748-9326/7/3/035703>
- Yi C, Wei S, Hendrey G (2014) Warming climate extends dryness-controlled areas of terrestrial carbon sequestration. *Sci Rep* 4:5472. <https://doi.org/10.1038/srep05472>
- Zaitchik BF, Evans JP, Geerken RA, Smith RB (2007) Climate and vegetation in the Middle East: interannual variability and drought feedbacks. *J Clim* 20(15):3924–3941. <https://doi.org/10.1175/JCLI4223.1>
- Zhang P, Jeong JH, Yoon JH, Kim H, Wang SS, Linderholm HW, Fang K, Wu X, Chen D (2020) Abrupt shift to hotter and drier climate over inner East Asia beyond the tipping point. *Science* 370(6520):1095–1099. <https://doi.org/10.1126/science.abb3368>